Available online at www.sciencedirect.com
SCIENCE DIRECT®
Journal of Crystal Growth 263 (2004) 143–147
JOURNAL OF CRYSTAL GROWTH
www.elsevier.com/locate/jcrysgro

Fe_xSi grown with mass-analyzed low-energy dual ion beam deposition

Lifeng Liu[a,*], Nuofu Chen[a,b], Fuqiang Zhang[a], Chenlong Chen[a], Yanli Li[a], Shaoyan Yang[a], Zhikai Liu[a]

[a] *Key Laboratory of Semiconductor Materials Science, Institute of Semiconductors, The Chinese Academy of Sciences, Beijing 100083, China*

[b] *National Laboratory of Micro-gravity, Institute of Mechanics, The Chinese Academy of Sciences, Beijing 100083, China*

Received 21 October 2003; accepted 25 November 2003
Communicated by M. Schieber

Abstract

Heavily iron-implanted silicon was prepared by mass-analyzed low-energy dual ion beam deposition technique. Auger electron spectroscopy depth profiles indicate that iron ions are shallowly implanted into the single-crystal silicon substrate and formed 35 nm thick Fe_xSi films. X-ray diffraction measurements show that as-implanted sample is amorphous and the structure of crystal is partially restored after as-implanted sample was annealed at 400°C. There are no new phases formed. Carrier concentration depth profile of annealed sample was measured by Electrochemical $C-V$ method and indicated that Fe_xSi film shows n-type conductivity while silicon substrate is p-type. The p–n junction is formed between Fe_xSi film and silicon substrate showing rectifying effect.

PACS: 81.05.Zx; 81.15.Hi; 82.80.P; 32.80.Ge

Keywords: A1. Auger electron spectroscopy; A1. X-ray diffraction; A3. Ion beam deposition; B2. Semiconducting silicon

1. Introduction

Diluted magnetic semiconductors (DMSs) are important in order to develop spin-controlled electronic devices and integrated magnetic device applications. The most extensively studied and most thoroughly understood materials of DMSs are $A^{II}_{1-x}Mn_xB^{VI}$ and $A^{III}_{1-x}Mn_xB^{V}$, in which Mn replaces a fraction of group II or III sublattices randomly [1–4]. On the other hand, Si thin films doped with magnetic transition metal impurities such as Fe, Co, Ni and Mn are also expected to be candidates for the DMSs [5,6]. Si-based DMSs would also be quite promising in the sense that spin-photonics devices can be integrated with existing Si large-scale-integrated-circuits (LSIs). Si-based DMSs have not been developed yet. Much research to the system of silicon and transition metals is about transition metal silicides [7–10]. Transition metal silicides have gained

*Corresponding author. Tel.: +86-10-8230-4569; fax: +86-10-8230-4469.
E-mail address: lfliu@red.semi.ac.cn (L. Liu).

0022-0248/$ - see front matter © 2003 Elsevier B.V. All rights reserved.
doi:10.1016/j.jcrysgro.2003.11.092

considerable attention as components in silicon-based microelectronics because of their favorable electrical properties and high thermal stability. The vast majority of transition metal silicides show metallic properties.

Heavily doping beyond the concentration of 1% of magnetic elements would be necessary in order to realize magnetic ions interactions in Si-based DMSs [11]. However, it is well known that the maximum solid solubility of transition metal ions at thermal equilibrium is very low. Therefore, the non-equilibrium doping process is necessary. Silicons heavily doped with transition metals such as iron, manganese and cobalt, have been successful grown by using gas-source molecular beam epitaxy (GSMBE) [11,12] laser-ablation molecular beam epitaxy (LAMBE) [13] and solid-phase diffusion [6]. The high-energy ions implantation is also a non-equilibrium doping process whose evident advantage is that the growth cost is low. However, the implanted high-energy ions will seriously destroy the crystal structure which needs high post-annealing temperature to restore, and the secondary phase is easy to form. In order to overcome the disadvantages of high-energy ions implantation, the low-energy ions can be applied, which can weaken the damage to crystal structure. It's expected to decrease the post-annealing temperature and suppress the formation of secondary phase.

In this paper, heavily iron-implanted silicon sample was prepared by mass-analyzed low-energy dual ion beam deposition with ion energy of 1000 eV. The as-implanted sample was annealed at 400°C. The atomic concentration of sample dependence on the depth was studied by Auger electron spectroscopy (AES) while the structure of the sample was analyzed by X-ray diffraction (XRD). The carrier concentration depth profile of annealed sample was studied by electrochemical $C-V$ method.

2. Material preparation

The sample was prepared by low-energy dual ion beam system, which can purify ions by mass selection in magnetic analyzer. The detailed description of the system is shown in Ref. [14]. p-Type silicon (1 1 1) was used as substrate. After cleaning with ethanol, acetone, HF and deionized water, the silicon was delivered into deposition chamber by a mechanical hand. The vacuum was $<10^{-6}$ Pa in the chamber. The substrate was annealed at 800°C for 30 min before growth in order to further eliminate the oxidation layer. The iron ion beams were produced by Bernas type ion source. Through mass-selection in magnetic filed and acceleration in electric filed, iron ions were implanted into silicon substrate with the energy of 1000 eV. The substrate was kept at room temperature during implanting. sample was implanted with doses of $3\times10^{17}\,cm^{-2}$ (sample A), a part of sample A was annealed at 400°C in an ultrahigh vacuum (sample B).

3. Measurements and analyses

3.1. Compositional analyses

The PHI-610/SAM AES system was employed for analyzing the compositional variation of the samples. Fig. 1 is the AES spectra at the sample surfaces, which show that there are iron, silicon, carbon and oxygen at the sample surfaces. The samples depth profiles are shown in Fig. 2. It can be seen that the concentrations of the oxygen and carbon are very high at the sample surfaces and decrease rapidly along the depth. The reason for existing of carbon is that the sample surfaces were contaminated after the samples were taken out from the growth chamber. The element oxygen is introduced by oxidation of iron after the samples were removed from the growth chamber. Sample B shows an out diffusion of iron toward the surface, favored by the damaged silicon structure. The iron atomic concentration of the sample A at the surface is 31% and increases to 46% at the surface of the annealed sample B. The relative concentrations of silicon and iron in the samples were kept to be identical after the depth of 35 nm. The film between the surface and the depth of 35 nm can be regarded as iron-implanted layer named Fe_xSi film. During the analyzed depth area, the relative concentration of silicon and iron in the sample B

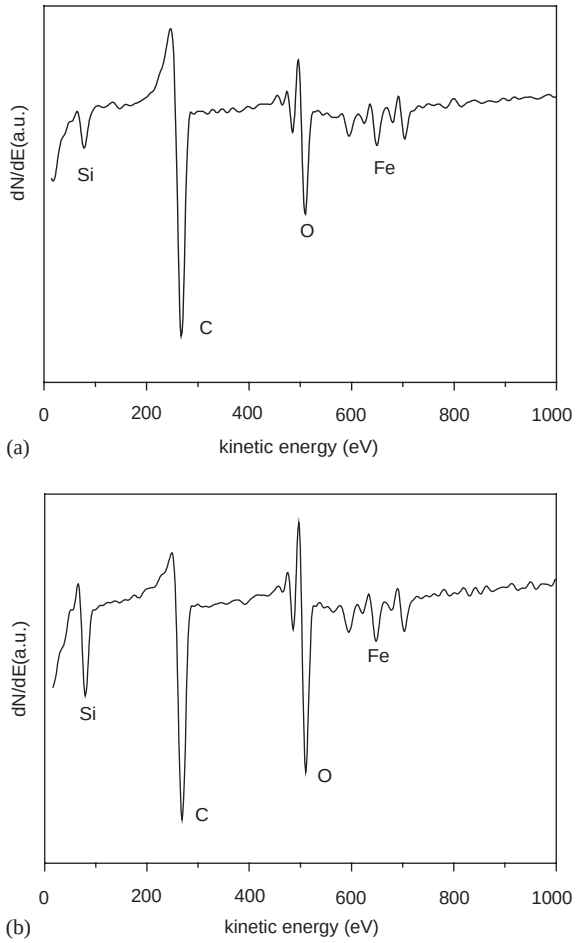

Fig. 1. Auger electron spectroscopy spectra at the surface of samples: (a) sample A and (b) sample B.

monotonically increase or decrease, indicating that there are not evident segregation of iron atoms in the annealed sample.

3.2. Structural analyses

XRD patterns of the samples were measured with a Rigaku diffractometer using CuKα radiation for structural analyses. The wide range XRD (20°–80°) patterns are shown in Fig. 3. The XRD spectra of samples A and B is Fig. 3(a) and (b), respectively. The structure of as-implanted sample A is destroyed by the heavily iron implanting and is amorphous. The crystal structure of sample B was partially restored after sample was annealed at

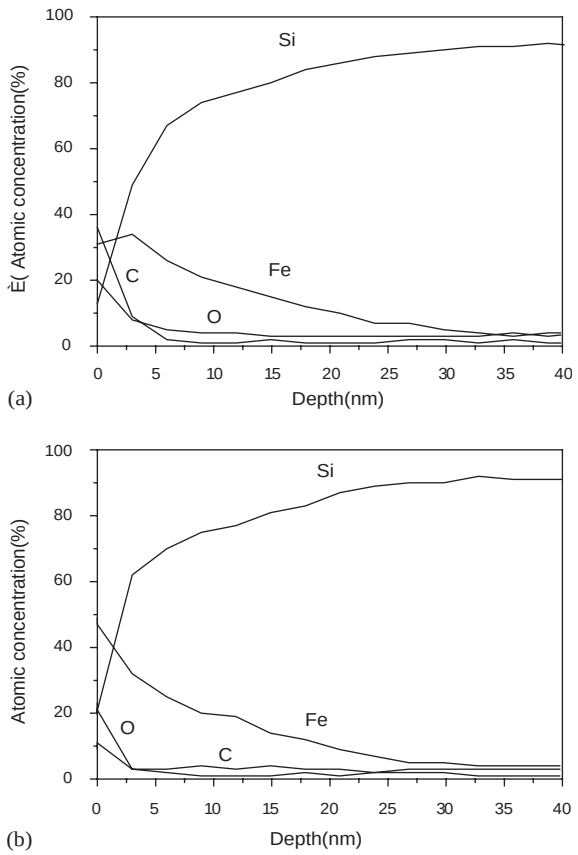

Fig. 2. Auger electron spectroscopy depth profile of samples: (a) sample A and (b) sample B.

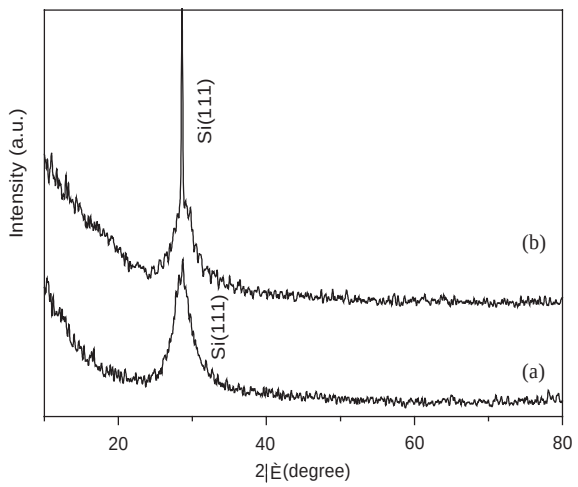

Fig. 3. X-ray diffraction spectra of samples: (a) sample A and (b) sample B.

400°C. It can be seen that there are no other diffraction peaks except for Si(1 1 1) in both samples A and B. We have carefully searched for secondary phases such as iron or iron silicides .However, none were observable. Then we measured the sample B by the X-ray double-crystal diffractometer. The X-ray diffractometer used is Philips X'pert-MRD (X'Pert Materials Research Diffractometer System) equipped with a multipurpose sample stage. The DXRD profile was measured by $\omega-2\theta$ scanning, in which again there is only Si(1 1 1) peak. The DXRD pattern is not shown here. These XRD dates show there are no new phases formed in samples. To study more carefully, the sample B was scanned slowly near 14.22° at the step of 0.0002°/s and the silicon substrate was also scanned for comparison. Fig. 4 shows the blown-up spectra of Fe_xSi(1 1 1) and Si(1 1 1). By comparison with the spectrum of Si(1 1 1), the spectrum of Fe_xSi is asymmetric and extended to low-angular side of the peak, which indicates that the lattice of silicon is expanded because silicon is implanted by the larger iron atoms and confirm the inhomogeneous concentration of iron in depth.

3.3. Electrical analyses

Carrier concentration depth profile of sample B was measured by the Bio-Rad PN4300 PN electrochemical $C-V$ system. Fig. 5 shows the carrier concentration depth profile. Electronic concentration at the sample surface is about $3.3\times10^{20}\,cm^{-3}$ and decreases rapidly along the depth to $5\times10^{16}\,cm^{-3}$ in the depth of 140 nm. Sample keeps the semiconducting property. Heavily iron-implanted silicon with p-type shows n-type conductivity. The p–n junction is formed between Fe_xSi film and silicon substrate. It is because that iron is the near mid-gap deep donor [15] and heavily iron doping causes the transformation of substrate conductivity. The interface of p–n junction could not be measured because iron atoms diffuse deeply in the annealed sample B

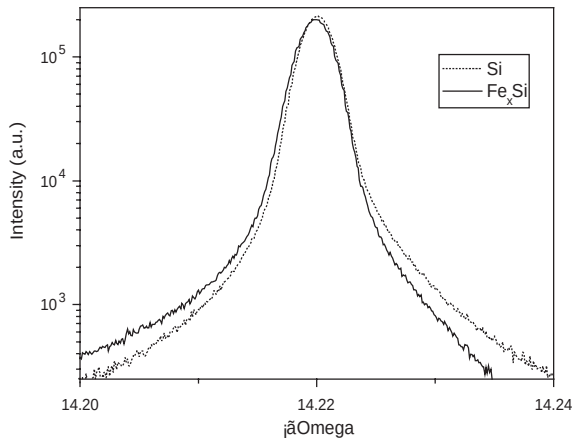

Fig. 4. X-ray double-crystal diffraction pattern ($\omega-2\theta$ scan) of sample B.

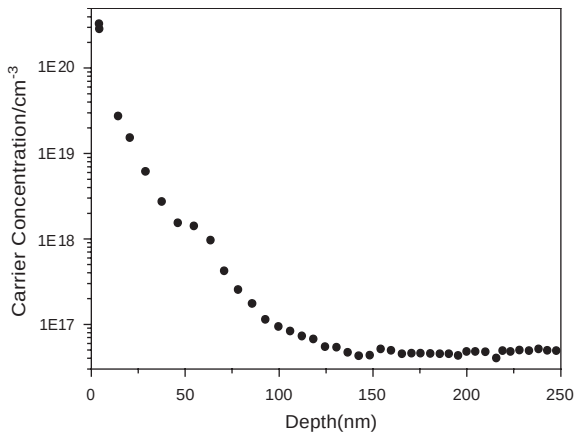

Fig. 5. Carrier concentration depth profile of sample B.

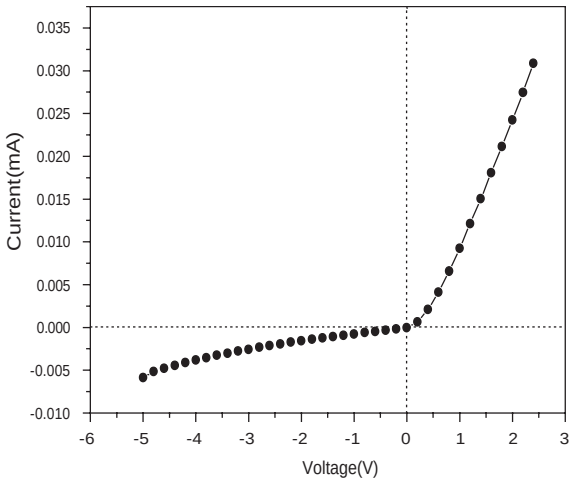

Fig. 6. Current–voltage curve of Fe_xSi/Si.

and silicon is difficult to erode. But the substrate was measured and attested to be p-type. The hole carrier concentration is about $2 \times 10^{15}\,cm^{-3}$. The current–voltage characteristic of the p–n junction was measured. It is showed in Fig. 6; the rectifying effect of sample is obvious. The result further confirms the formation of p–n junction between the Fe_xSi film and silicon substrate.

4. Summary

Semiconducting Fe_xSi sample was obtained by mass-analyzed low-energy dual ion beam deposition with low-iron ion energy of 1000 eV and a high dose of $3 \times 10^{17}\,cm^{-2}$ at room temperature. The structure of as-implanted sample is amorphous. Sample was annealed at 400°C and partially crystallized. There is no new phase formed both in as-implanted sample and in annealed sample. Fe_xSi film shows n-type conductivity while silicon substrate is p-type. The p–n junction is formed between Fe_xSi film and silicon substrate showing rectifying effect.

Acknowledgements

This work was partially supported by the National Natural Science Foundation of China (Grant No. 60176001, 60390072) and Special Funds for Major State Basic Research Projects of China (Grant No. 20000365, 2002CB311905).

References

[1] H. Ohno, A. Shen, F. Matsukura, A. Oiwa, A. Endo, S. Katsumoto, Y. Iye, Appl. Phys. Lett. 69 (1996) 363.
[2] M.L. Reed, N.A. El-Masry, H.H. Stadelmaier, M.K. Ritums, M.J. Reed, C.A. Parker, J.C. Roberts, S.M. Bedair, Appl. Phys. Lett. 79 (2001) 3473.
[3] A. Haury, A. Wasiela, A. Arnoult, J. Cibert, S. Tatarenko, T. Dietl, Y. Merle dAubigné, Phys. Rev. Lett 79 (1997) 511.
[4] X. Liu, U. Bindley, Y. Sasaki, J.K.J Furdyna, Appl. Phys. 91 (2002) 2859.
[5] E. Kulatov, H. Ohta, H. Nakayama, T. Nishino, Proceedings of the Fourth Symposium on the Physics and Application of Spin-Related Phenomena in Semiconductors, Sendai, 1998, p. 126.
[6] S. Abe, H. Nakayama, T. Nishino, H. Ohta, S. Iida, J. Crystal Growth. 210 (2000) 137.
[7] H. Lange, Phys. Stat. Sol. B. 201 (1997) 3.
[8] Y. Gao, S.P. Wong, W.Y. Cheung, G. Shao, K.P. Homewood, Appl. Phys. Lett. 83 (2003) 638.
[9] J.-L. Yang, N.-F. Chen, Zh.-K. Liu, Sh.-Y. Yang, Ch.-L. Chai, M.-Y. Liao, H.-J. He, J. Crystal Growth 226 (2001) 517.
[10] D.H. Tassis, C.L. Mitsas, T.T. Zorba, C.A. DiMitriadis, O. Valassiades, D.I. Siapkas, M. Angelakeris, P. Poulopoulos, N.K. Flevaris, G. Kiriakidis, J. Appl. Phys. 80 (1996) 962.
[11] H. Nakayamaa, H. Ohtab, E. Kulatov, Physica B 0.302–303 (2001) 419.
[12] H. Nakayama, H. Ohta, E. Kulatov, Thin Solid Films 395 (2001) 230.
[13] S. Abe, Y. Nakasima, S. Okubo, H. Nakayama, T. Nishino, H. Yanagi, H. Ohta, S. Appl. Surf. Sci. 142 (1999) 537.
[14] F.-G. Qin, X.-M. Wang, Z.-K. Liu, et al., Rev. Sci. Instrum. 62 (1991) 2322.
[15] H. Nakashima, T. Sadoh, H. Kitagawa, K. Hashimoto, Mater. Sci. Forum 143–144 (1994) 761.